JACS
JOURNAL OF THE AMERICAN CHEMICAL SOCIETY

Article

pubs.acs.org/JACS

New Functional Handle for Use as a Self-Reporting Contrast and Delivery Agent in Nanomedicine

Mathew P. Robin,[†] Anne B. Mabire,[†] Joanne C. Damborsky,[‡] Elizabeth S. Thom,[‡] Ursula H. Winzer-Serhan,[‡] Jeffery E. Raymond,*[,§,∥] and Rachel K. O'Reilly*[,†]

[†]Department of Chemistry, University of Warwick, Library Road, Coventry CV4 7AL, United Kingdom

[‡]Department of Neuroscience and Experimental Therapeutics, College of Medicine, Health Sciences Center, Texas A&M University System, Bryan, Texas 77807, United States

[§]Department of Chemistry and [∥]Laboratory for Synthetic-Biologic Interactions, Texas A&M University, College Station, Texas 77842-3012, United States

Supporting Information

ABSTRACT: The synthesis and photophysical characterization of a chromophore-bridged block copolymer system is presented. This system is based on a dithiomaleimide (DTM) functional group as a highly emissive functionality which can readily be incorporated into polymeric scaffolds. A key advantage of this new reporter group is its versatile chemistry, ease of further functionalization, and notably small size, which allows for ready incorporation without affecting or disrupting the self-assembly process critical to the formation of core−shell polymeric contrast and drug delivery agents. We demonstrate the potential of this functionality with a diblock system which has been shown to be appropriate for micellization and, when in the micellar state, does not self-quench. The block copolymer is shown to be significantly more emissive than the lone dye, with a concentration-independent emission and anisotropy profile from 1.5 mM to 0.15 μM. An emission lifetime and anisotropy decay comparison of the block copolymer to its micelle displays that time-domain fluorescence lifetime imaging (FLIM) is able to rapidly resolve differences in the supramolecular state of this block−dye−block polymer system. Furthermore, the ability to resolve these differences in the supramolecular state means that the DTM micelles are capable of self-reporting when disassembly occurs, simply by monitoring with FLIM. We demonstrate the great potential for in vitro applications that this system provides by using FLIM to observe micelle disassembly in different vascular components of rat hippocampal tissue. In total this system represents a new class of in-chain emitter which is appropriate for application in quantitative imaging and the tracking of particle degradation/disassembly events in biological environments.

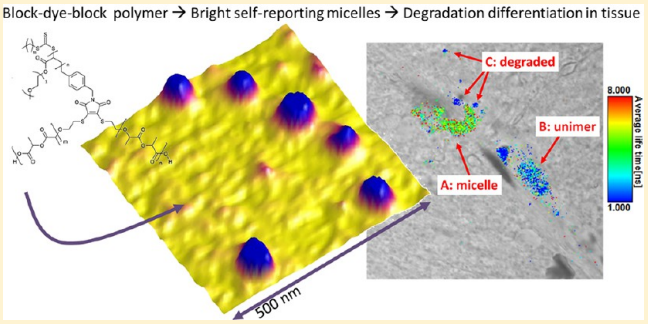

INTRODUCTION

There has been much recent interest in the use of core−shell polymeric nanoparticles as contrast agents[1] and in-cell delivery platforms in nanomedicine.[2] Strategies for incorporating contrast and bioactive media into these systems have included tethering,[3] cross-linking,[4] and noncovalent interactions.[5] These have included processes at all three particle regions (core,[6] shell,[7] and surface[8]), but little has been done at the core−shell interface. We propose this region is of particular interest given its environment-shielded nature compared to the surface or shell domain and distinct spatially separated location from encapsulants loaded into the interior of the scaffold. These features are key to ensuring that the emissive properties of the reporter are unaffected by local changes within the scaffold or its immediate surroundings and instead can be reliably correlated to specific whole-system events.

Common issues with conventionally labeled systems, in application, include the inability to readily observe how incubated molecules interact with the host and often no conclusive way to track particle degradation in vitro as it occurs. There is often ambiguity regarding the location of the binding molecule and its mobility in the micellar host, both for contrast agents and with pharmacological payloads. Another problem arising from encapsulation is decreased emission from loaded contrast agents, through either probe−polymer interactions or probe−probe self-quenching events.[9] Furthermore, it is known that incorporation of an emissive handle, often a large hydrophobic molecule, can lead to changes in scaffold size, stability, and even encapsulation potential due to surface modification effects.[2] Thus, new methods for the facile and nondisruptive labeling of nanostructures are required.

One solution to these particular difficulties is the formation of a reporter group system which can be readily incorporated

Received: April 10, 2013

   dx.doi.org/10.1021/ja403587c | J. Am. Chem. Soc. XXXX, XXX, XXX−XXX

Scheme 1. (a) Synthesis of Dual ROP/RAFT Initiator 1, (b) Synthesis of Amphiphilic Copolymer 2 by Sequential ROP and RAFT Polymerization, (c) Self-Assembly of 2 To Give Spherical Micelles 2M, and (d) Synthesis of Small-Molecule DTMs 3 and 4

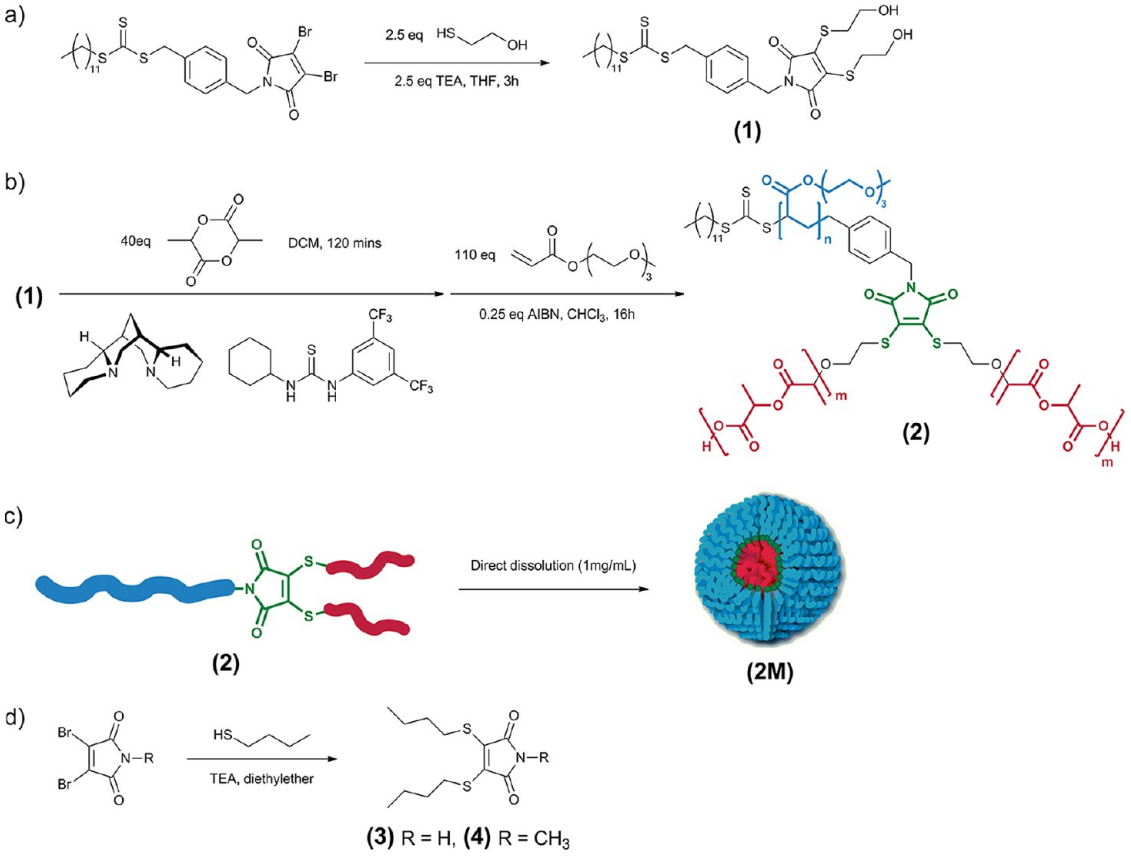

into the polymeric scaffold and used as an emissive reporter with a nonambiguous location in the nanostructure. For this study, we have selected the core−shell interface. In our previous work, we have displayed the versatility of dithiomaleimides (DTMs) as a new highly emissive fluorophore for protein and polymer labeling.[10] In this study we have explored the incorporation of this new system directly into a block copolymer scaffold, using the facile and well-established ring-opening polymerization (ROP)[11] and reversible addition−fragmentation chain transfer (RAFT) polymerization[12] methods. Indeed, we highlight how this functional handle can be used as a reporter group to track the micellar state and also allow for facile in situ particle tracking using its built-in bright fluorescence and self-reporting properties. This highly emissive and self-reporting system offers great potential for nanomedicine applications. Furthermore, given the ease of synthesis and ready incorporation into polymeric systems, we propose this new probe also has potential in a range of sensing and tracking applications.

RESULTS AND DISCUSSION

Polymer Synthesis. Our investigations have focused on the incorporation of DTM functionality and its exploration as a bright and emissive probe in both polymers and amphiphilic polymer self-assembled structures. Positioning the DTM unit at the core−shell interface required that the hydrophobic and hydrophilic blocks of the amphiphile were polymerized from either end of this functional group by two orthogonal polymerization techniques (Scheme 1). To achieve this objective, we utilized a DTM-containing dual ROP/RAFT initiator, **1**, which we have previously shown to be highly tolerant to polymerization conditions.[10] ROP using a thiourea/(−)-sparteine organocatalyst system[13] could first be initiated from the hydroxyl groups on the S substituents of the DTM unit to form the hydrophobic poly(D,L-lactide) block. Then RAFT polymerization from the trithiocarbonate attached through the N of the DTM unit afforded the hydrophilic triethylene glycol monomethyl ether acrylate (TEGA) block. The resultant Y-shaped amphiphilic block copolymer, **2**, was subsequently characterized using ^{1}H NMR spectroscopy and size exclusion chromatography (SEC) ($M_{n,NMR}$ = 28.4 kg·mol^{-1}, $Đ_{SEC}$ = 1.22, Figures S1 and S3, Supporting Information). To assist with the emissive characterization of the new materials, two further small-molecule DTMs were prepared, **3** and **4**. It should be noted that N-Alkylation (**4**) had only a minor effect on the fluorescence properties (see the Supporting Information), so only **3** will be discussed in detail below.

Micelle Assembly. Self-assembly of polymer **2** into spherical micelles was achieved using direct dissolution methods to afford a solution of micelles (**2M**) at 1 mg/mL. The number-average diameter was found to be 23 nm via dynamic light scattering (DLS), with a polydispersity index (PDI) of 0.17 (Figure S4, Supporting Information). To confirm a micellar structure, atomic force spectroscopy (AFM) was used to observe the micelles on a glass substrate. A micrograph of a typical sampling with a height profile is presented in Figure 1. While the micelles were not stable enough to be imaged on a

dx.doi.org/10.1021/ja403587c | J. Am. Chem. Soc. XXXX, XXX, XXX−XXX

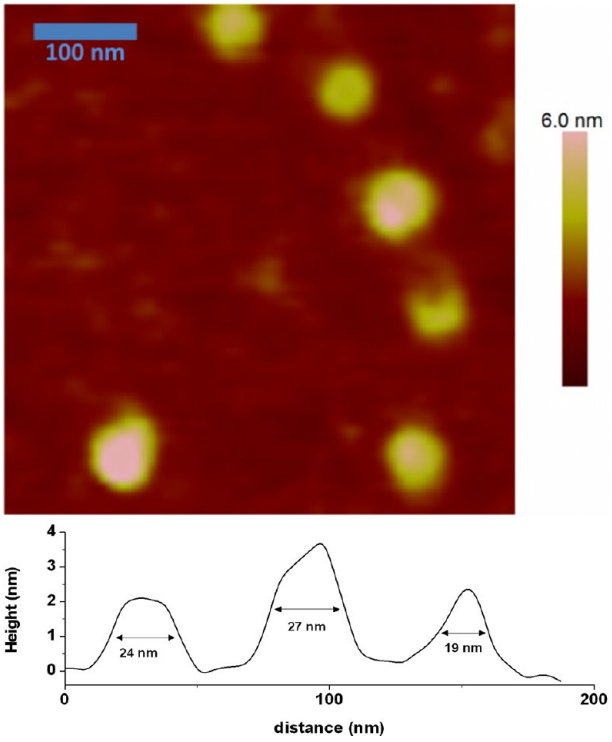

Figure 1. Solution-phase AFM micrograph of micelles **2M** imaged on a glass substrate and cross-section depicting typical micelle sizes.

high-energy surface (mica), which they immediately coated, the AFM images presented from solution-phase imaging on a lower energy surface (glass) were comparable in diameter to the DLS results. Furthermore, the micelles were also imaged in the dried state on a low-contrast graphene oxide support by transmission electron microscopy (TEM) without staining,[14] which confirmed an average diameter of 19.1 ± 2.1 nm (Figure S5, Supporting Information).

Steady-State Fluorescence and Emission Anisotropy. Both species **2** and **3** possessed similar UV−vis and excitation spectra, with maxima near 403 nm. Steady-state emission spectra for **2** and **3** are presented in Figure 2 from 405 nm excitation. Quantum yield measurements for **2** (10 μM) in methanol resulted in a Φ_{PL} of 0.343 ± 0.004. In comparison, the ca. 30-fold less emissive **3** (12 μM) possessed a Φ_{PL} of 0.011 ± 0.002. In particular, the micelle emission efficiency compares very favorably to other common fluorescent labels, Φ_{PL} of 0.02−0.90,[15] without suffering from self-quenching, despite a dye concentration in the micelle which can be calculated from DLS R_h at ca. 0.05 M. The authors attribute this increased emission to the polymeric substituents preventing both solvent/collisional quenching effects and self-quenching, though a planarization effect of the polymer substituents is not entirely ruled out. To observe the effect of concentration on emissivity, a dilution study was also performed (Figure 2). It can be seen from these integrated emission intensities that emission from **3** scales similarly to that of most self-quenching fluorophores,[9] while the micelle forming **2** possesses a relatively flat emission profile over 3 orders of magnitude of concentration.

To confirm the supramolecular state of **2** during this relatively low dependence of emission on concentration, steady-state anisotropy spectroscopy was performed. While the anisotropy for emission from **3** remained flat with regard to

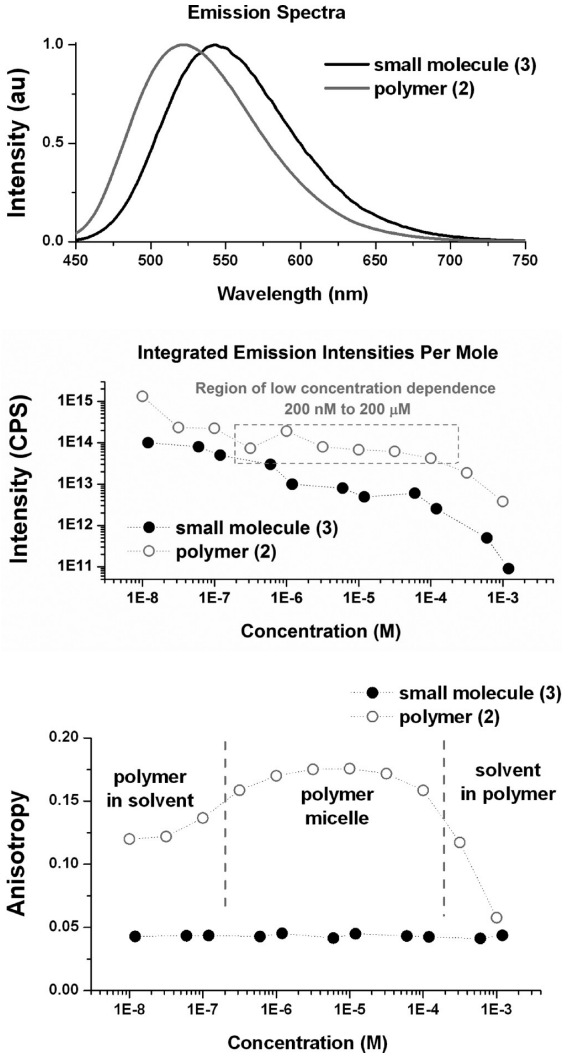

Figure 2. Steady-state emission spectra and concentration-based emissivity and emission anisotropy for small-molecule **3** and polymer **2**.

concentration at r = 0.043 ± 0.001, the anisotropy of **2** changed significantly over the same concentration range (Figure 2). At high concentrations, anisotropy for **2** approaches that of **3**, which the authors assign to a solvent-in-polymer character where **2**-to-**2** FRET and hopping events may lead to an overall less polarized emission.[16] In the region of uniform emissivity, anisotropy is highest (0.17), typical of a polymer micelle state where a chromophore's tumbling is reduced by incorporation into a structure where mass and volume have increased and collisional quenching with solvent is inhibited.[17] At low concentrations, anisotropy decreases to ca. 0.12 and should be taken to represent a response approaching that of the isolated polymer-in-solvent state. The fact that anisotropy does not decrease in the intermediate concentrations where a micellar state exists is particularly telling. A subtly to note is that the in-micelle local dye concentration is significantly higher than the highest sample concentration investigated (1 mM). Detailed excellently in a topical review by Olaya-Castro and Scholes,[18] increased emissivity and anisotropy from chromophore-dense assemblies are an indication of coherent energy transfer (ET) events in supramolecular structures where regular or semiordered geometries exist between substituents. How-

dx.doi.org/10.1021/ja403587c | J. Am. Chem. Soc. XXXX, XXX, XXX−XXX

ever, without proximal ordering, these effects are not observed in disordered solutions, even at high concentrations. In this second case, without ordered and constrained architecture, the more conventional ET regime dominates with all of the typical effects of increased concentration (such as decreased anisotropy, quenching, and/or reabsorption) manifesting in turn. In all, both emission and anisotropy trends provide a method for distinguishing between supramolecular conditions via steady-state assessment and point to a system where time-resolved spectra may be particularly pointed in resolving changes in state.

Fluorescence Lifetime and Anisotropy Decay. To assess the viability of this polymer system for fluorescence lifetime imaging microscopy (FLIM), solution-state time-correlated single-photon counting (TCSPC) was performed to determine emission and anisotropy decay profiles. A polymer-in-solvent (**2S**, 10 nM), polymer micelle (**2M**, 1 μM) and chromophore solution (**3X**, 1.2 μM) were assessed with a pulsed 405 nm diode laser (135 ps fwhm), and resultant emission decay and anisotropy decay spectra are presented in Figure 3 with kinetic information in Table 1. All species

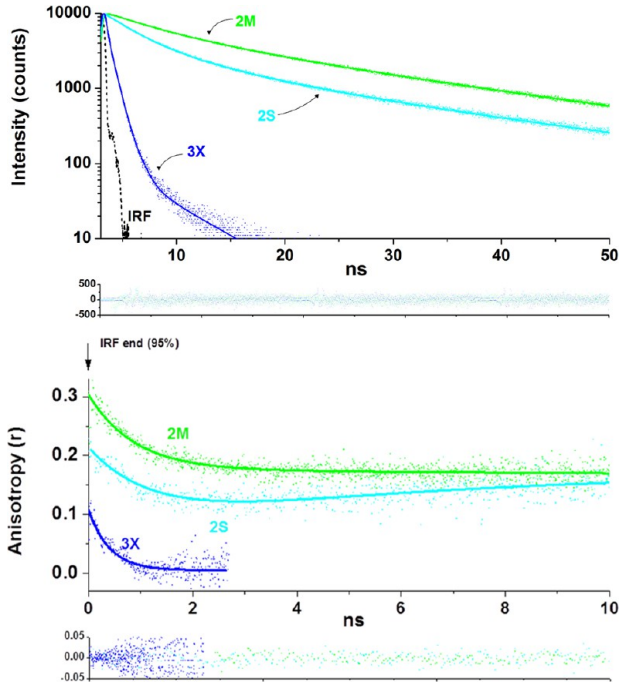

Figure 3. Fluorescence lifetime (top) and anisotropy decay spectra (bottom) for **2M**, **2S**, and **3X** with residuals.

consistently displayed three components to decay after deconvolution. The lone chromophore **3X** decays almost immediately, with two near-ultrafast lifetimes comprising the majority of decay and one longer decay of ca. 5 ns. The significance of this result can be assigned and summarized as follows: (i) the shortest decays can reasonably be assigned to nonemissive aggregation and solvent-collision effects[19] and (ii) the longer lifetime as an intrinsic relaxation event for this family of emitter, observed also as the τ_1 decay in the **2** series. However, the critical comparison, in terms of application, is of the micellar system **2M** and the solvated polymer **2S** as these differences will be key to observation of particle disassembly in vitro and in vivo. Perhaps easiest to implement is a direct comparison of average lifetimes ($\tau_{av,A}$ = 7.6–13 ns, $\tau_{av,I}$ = 15–20 ns) or emission half-lives, though any of the component extractions are sufficiently different to detect a change in state for this system.

Often even more sensitive to the local environment, anisotropy decay kinetics can also be a powerful tool for the assessment of super-, supra-, and macromolecular states.[16,19,20] For **3X**, decay from $r(0)$ = 0.11 to $r(0)$ = ca. 0 occurs immediately during the first nanosecond. Comparison of **2S** and **2M** provides such contrast in anisotropy kinetic character that all components of the fitting can be used to discriminate between the micellar state and the unimer. Most telling is the apparent anisotropy recovery observed in **2S**. This rise is assigned to the emission decay of lower anisotropy states, which results in a greater expression of more anisotropic states, possibly quasi-micellar or aggregate interactions.[16,21] In conjunction with a larger steady-state anisotropy in **2M** as compared to **2S**, these spectra display that the total anisotropy decay profile and all of the extractions are viable signaling channels for monitoring a transition from a micellar state to a disassembled/degraded one.

Taking all emission and anisotropy lifetime information in total, a picture emerges relating kinetics to the polymer assembly state with final assignments as follows: (i) τ_1 in the **2** series and τ_3 in **3X** are assigned to intrinsic lifetimes of the species,[20,22] (ii) longer lifetimes and higher amplitudes for τ_2 and τ_3 for **2M** are the result of better fluorophore protection when compared to **2S**,[16] (iii) fast anisotropy decay in **2M** suggests the possibility of coherent effects from localized, similarly oriented dye bridges at the core–shell interface,[19,20] and (iv) the long anisotropy decay in **2M** informs as to the time scale at which micellar tumbling occurs. For a detailed discussion of the emission lifetime and anisotropy decay for **2P** see the Supporting Information.

FLIM. To display the viability of self-assembled nanoparticles as self-reporting agents for nanomedicine applications, **2S** and **2M** were cast onto glass and the films (**2S′** and **2M′**) inspected by FLIM (excitation 405 nm, 450 nm long-pass collection). The resulting images and spectral data are presented in Figure 4. FLIM images indicate that both systems possess extensive micellization in the solid state. However, polymer scarcity on deposition of **2S**, and a lack of micelle structure predeposition, results in large droplet-like structures and a film background of unassembled polymer. While resolution limits preclude observation of nanoscale micelles in these systems, it is reasonable that the majority of the nanoscale micelles remain in the casting of **2M** despite some larger (1 μm) structures. Direct lifetime tail fittings of the entire field of view are presented in Table 1. Again, observing the contrast in signals, a poignant difference in contributions to signal for the short lifetime and longer two lifetimes exist, with **2M′** possessing a significantly larger contribution to signal from longer lived states. Component lifetimes are also longer for **2M′** in all cases, as is the half-life. Comparing the average arrival time of emission and the lifetime extraction histograms (fast-FLIM signal) for both systems reveals that, even without formal emission fitting, total photon arrival times per pixel are readily capable of resolving the difference in average supramolecular state of each system (Figure 4). This ability to differentiate between states is of particular importance in terms of end-use application in translational and pharmacological studies. To summarize, the results we detail here mean that in future work with DTM functional nanoparticles it will not be necessary for expert care to be given to spectral analysis. Rather, it should be possible to

dx.doi.org/10.1021/ja403587c | J. Am. Chem. Soc. XXXX, XXX, XXX–XXX

Table 1. Emission Lifetime and Anisotropy Kinetics for Solution- and Solid-State Systems

	Lifetime								
	A_1	τ_1 (ns)	A_2	τ_2 (ns)	A_3	τ_3 (ns)	$\tau_{av,I}$ (ns)	$\tau_{av,A}$ (ns)	$t_{1/2}$ (ns)
2S	0.66	3.0 ± 0.1	0.29	9.1 ± 0.2	0.15	25.2 ± 0.2	15	7.6	6.9
2M	0.45	5.1 ± 0.2	0.48	17.5 ± 0.1	0.07	39.4 ± 0.5	20	13	10.9
3X	0.68	0.31 ± 0.01	0.31	0.77 ± 0.1	0.01	5.2 ± 0.1	1.0	0.50	3.7
	Anisotropy								
	A_1	τ_1 (ns)	A_2	τ_2 (ns)	$r(0)^a$	$r(\text{inf})^b$	$\langle r \rangle^c$		
2S	0.098	1.3 ± 0.3	0.048^{rise}	0.77 ± 0.1	0.22	0.17	0.12		
2M	0.132	0.8 ± 0.1	0.034	50 ± 15	0.31	0.144	0.17		
3X	0.105	0.40 ± 0.02			0.11	0.005	0.04		
	FLIM								
	A_1	τ_1 (ns)	A_2	τ_2 (ns)	A_3	τ_3 (ns)	$\tau_{av,I}$ (ns)	$\tau_{av,A}$ (ns)	$t_{1/2}$ (ns)
2S′	0.27	2.2 ± 0.1	0.32	13.3 ± 0.2	0.41	31.0 ± 0.2	26	17	5.4
2M′	0.08	2.3 ± 0.2	0.43	16.5 ± 0.1	0.49	44 ± 1	37	29	6.9

[a] $r(0)$ is the anisotropy fit value after 95% of instrument response function (IRF), with the difference between $r(0)$ and 0.4 taken as the ultrafast decay amplitude. [b] $r(\text{inf})$ is the asymptotic anisotropy reached by 95% of decay intensity. [c] $\langle r \rangle$ is the steady-state anisotropy at emission maxima with 405 nm excitation.

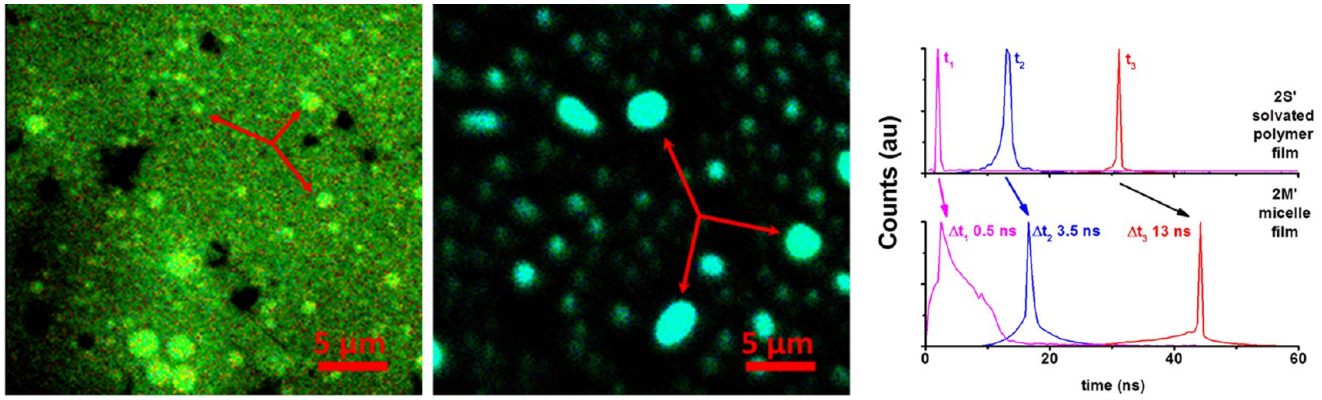

Figure 4. FLIM of cast **2M′** (left) and **2S′** (middle) with droplet-like microstructures indicated by arrows and fast-FLIM lifetime extraction histograms (right) from average photon arrival times.

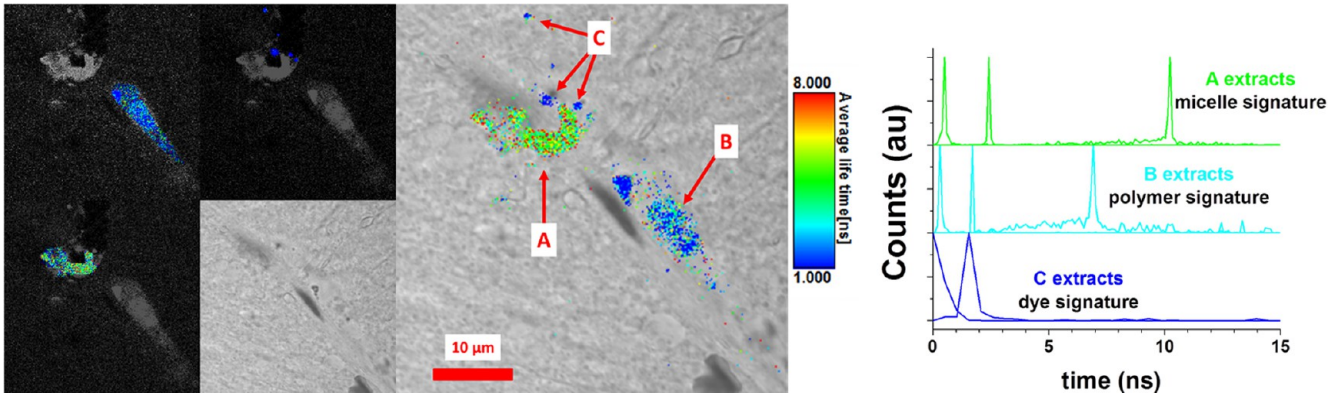

Figure 5. FLIM of **2M** in rat hippocampal tissue with fast-FLIM emission lifetime extractions for the clotting region (A), vascular tissue (B), and blood cells (C).

readily generate biological protocols for the use of this system in a fashion that does not require extensive and overtly time-consuming analysis of the decay spectra. As a demonstration of the great potential these self-reporting micellar contrast agents possess, we investigated FLIM of the particles in rat hippocampal tissue.

FLIM in Rat Hippocampal Tissue. It is known that polymeric nanoparticles which have not been tailored to penetrate the blood–brain barrier tend to have a variety of interactions with vascular tissues and fluids which inhibit transport into neuronal tissue.[2,23] To provide a proof-of-principle test in vitro, a cross-section of living rat hippocampal tissue was subjected to ca. 0.1 mL of 10 mg/mL polymer micelles in phosphate-buffered solution for 1 h, fixed with ethanol, and then imaged via FLIM. It was found that the micelles and degradation products could be found in three

dx.doi.org/10.1021/ja403587c | J. Am. Chem. Soc. XXXX, XXX, XXX–XXX

forms in the tissue, identified by their respective fluorescence lifetimes, with all states associated with vascular tissue components (Figure 5). In clotted regions (A), it could be observed that micellar (**2M**) emission was retained, while on the vascular wall (B), a shorter lifetime non-micellar polymer (**2S**) emission can be observed. Emission from blood cells exposed to the micelles (C) displayed the shortest lifetimes. While this may be the result of heme-group emission,[24] the longer lifetime components of the emission profile do not support this theory and suggest instead that degraded polymer may have bound to the cells, resulting in emission similar to that of the solution-phase dye (**3X**). Indeed, emission decay for the C region overlays almost exactly with that of **3X**, with τ_{av} = 1.1 and 1.0 ns, respectively (Figure S11, Supporting Information).

Application of Block–Dye–Block Emitters as Quantitative Contrast Agents and Self-Reporters. The advantage of being able to use a concentration-independent emitter as part of a diblock micelle or cross-linked nanoparticle relates to the generation of a venue for quantitative microscopic techniques in assessing nanomedicine delivery platforms. In short, without ambiguities regarding the state/location of the emitter, it becomes possible to perform cellular imaging where emission intensity is truly an indication of particle density. Similarly, for the determination of small-molecule location and loading/unloading kinetics in a polymeric nanoparticle, it becomes possible to use the FRET signal to or from the built-in chromophore to track molecules moving across the core–shell interface. Given the differences in emission anisotropy and lifetime, these materials may be ideal candidates for FLIM, anisotropy or anisotropy decay imaging of particle incorporation, and degradation both in vitro and in vivo. Lastly, noting the various gross differences in total and component decay parameters (Table 1), an array of possibilities exist for developing biological protocols that provide unambiguous answers regarding micelle location and its supramolecular state (micellar polymer, non-micellar polymer, or degraded).

In practice, we suggest use of the fast-FLIM signal, fast-FLIM component signal, or a gating technique[25] for analysis when using FLIM for degradation/disassembly studies in these venues. By gating, the authors refer to selecting the temporal region where **2M** emission intensities have the highest ratio of difference for analysis. This bypasses the arduous assessment of similar fast-lifetime emission components and allows one to look at trends in specific temporal regions where micelle emission and free polymer emission are distinctly different.

CONCLUSIONS

We present the full synthesis and photophysical properties of a polymeric emitter capable of self-assembly into bright self-reporting nanoparticles. The block–dye–block strategy presented here is the first of a new platform chemistry for generating self-reporting materials for nanomedicine through the incorporation of a specific dithiomaleimide functional group. Spectral analysis of the concentration dependence of the fluorescent polymer shows that supramolecular structuring controls emissivity, emission polarization, and lifetime. This new probe with self-reporting capabilities can be readily incorporated into polymeric nanostructures and, given its small size, can be considered non-invasive. Application methods are both shown and discussed throughout this work to best utilize the unique signaling capabilities of this system. In addition to being shown as a viable self-reporting system for solid-state applications and in-tissue studies, the "at the core–shell interface" strategy provides a route to potentially tracking explicit loading and unloading kinetics from changes in the spectral signature of the DTM from transient species crossing to and from the core.

ASSOCIATED CONTENT

Supporting Information

Experimental section, characterization data (NMR, SEC, DLS, TEM), fluorescence analysis of **4**, and discussion of high-concentration (**2P**) FLIM. This material is available free of charge via the Internet at http://pubs.acs.org.

AUTHOR INFORMATION

Corresponding Author

jeffery.raymond@mail.chem.tamu.edu; r.k.o-reilly@warwick.ac.uk

Notes

The authors declare no competing financial interest.

ACKNOWLEDGMENTS

We graciously thank the following agencies for ongoing support of this project: Office of Naval Research (Grant N00014-10-1-0527), Welch Foundation (Grant A-0001), Engineering and Physical Sciences Research Council, European Science Foundation, and the University of Warwick Erasmus program. We also thank Karen L. Wooley (Texas A&M University) for the use of laboratory space and preparative equipment.

REFERENCES

(1) Xiong, H.-M.; Xu, Y.; Ren, Q.-G.; Xia, Y.-Y. *J. Am. Chem. Soc.* **2008**, *130*, 7522.
(2) Elsabahy, M.; Wooley, K. L. *Chem. Soc. Rev.* **2012**, *41*, 2545.
(3) Zhu, M.-Q.; Zhu, L.; Han, J. J.; Wu, W.; Hurst, J. K.; Li, A. D. Q. *J. Am. Chem. Soc.* **2006**, *128*, 4303.
(4) Sun, G.; Berezin, M. Y.; Fan, J.; Lee, H.; Ma, J.; Zhang, K.; Wooley, K. L.; Achilefu, S. *Nanoscale* **2010**, *2*, 548.
(5) Lee, V. Y.; Havenstrite, K.; Tjio, M.; McNeil, M.; Blau, H. M.; Miller, R. D.; Sly, J. *Adv. Mater.* **2011**, *23*, 4509.
(6) Tian, Z.; Li, A. D. Q.; Hu, D. *Chem. Commun.* **2011**, *47*, 1258.
(7) Xu, J.; Sun, G.; Rossin, R.; Hagooly, A.; Li, Z.; Fukukawa, K.-i.; Messmore, B. W.; Moore, D. A.; Welch, M. J.; Hawker, C. J.; Wooley, K. L. *Macromolecules* **2007**, *40*, 2971.
(8) Li, Q.; Zhang, L.; Bai, L.; Zhang, Z.; Zhu, J.; Zhou, N.; Cheng, Z.; Zhu, X. *Soft Matter* **2011**, *7*, 6958.
(9) Anthony, O.; Zana, R. *Langmuir* **1996**, *12*, 1967.
(10) Robin, M. P.; Wilson, P.; Mabire, A. B.; Kiviaho, J. K.; Raymond, J. E.; Haddleton, D. M.; O'Reilly, R. K. *J. Am. Chem. Soc.* **2013**, *135*, 2875.
(11) Dove, A. P. *Chem. Commun.* **2008**, *2008*, 6446.
(12) Moad, G.; Rizzardo, E.; Thang, S. H. *Aust. J. Chem.* **2012**, *65*, 985.
(13) Pratt, R. C.; Lohmeijer, B. G. G.; Long, D. A.; Lundberg, P. N. P.; Dove, A. P.; Li, H.; Wade, C. G.; Waymouth, R. M.; Hedrick, J. L. *Macromolecules* **2006**, *39*, 7863.
(14) Patterson, J. P.; Sanchez, A. M.; Petzetakis, N.; Smart, T. P.; Epps, T. H., III; Portman, I.; Wilson, N. R.; O'Reilly, R. K. *Soft Matter* **2012**, *8*, 3322.
(15) Langhals, H.; Karolin, J.; Johansson, L. B.-Å. *J. Chem. Soc., Faraday Trans.* **1998**, *94*, 2919.
(16) Beija, M.; Fedorov, A.; Charreyre, M.-T.; Martinho, J. M. G. *J. Phys. Chem. B* **2010**, *114*, 9977.
(17) Yildiz, I.; Impellizzeri, S.; Deniz, E.; McCaughan, B.; Callan, J. F.; Raymo, F. M. *J. Am. Chem. Soc.* **2011**, *133*, 871.

(18) Olaya-Castro, A.; Scholes, G. D. *Int. Rev. Phys. Chem.* **2011**, *30*, 49.
(19) Wang, Y.; Goodson, T., III. *J. Phys. Chem. B* **2007**, *111*, 327.
(20) Varnavski, O.; Goodson, T., III; Sukhomlinova, L.; Twieg, R. *J. Phys. Chem. B* **2004**, *108*, 10484.
(21) Qin, A.; Lam, J. W. Y.; Tang, B. Z. *Prog. Polym. Sci.* **2012**, *37*, 182.
(22) (a) Lahankar, S. A.; West, R.; Varnavski, O.; Xie, X. B.; Goodson, T.; Sukhomlinova, L.; Twieg, R. *J. Chem. Phys.* **2004**, *120*, 337. (b) Yoo, H.; Yang, J.; Nakamura, Y.; Aratani, N.; Osuka, A.; Kim, D. *J. Am. Chem. Soc.* **2009**, *131*, 1488.
(23) Mailänder, V.; Landfester, K. *Biomacromolecules* **2009**, *10*, 2379.
(24) Chaudhuri, S.; Chakraborty, S.; Sengupta, P. K. *Biophys. Chem.* **2011**, *154*, 26.
(25) Huang, K. W.; Marti, A. A. *Anal. Chem.* **2012**, *84*, 8075.